SIMULATION OF MULTISCALE INDUSTRIAL SOLIDIFICATION PROBLEM UNDER INFLUENCE OF ELECTROMAGNETIC FIELD BY MESHLESS METHOD

B. ŠARLER[1,2], A. Z. GUŠTIN[1], V. HATIĆ[1], N. KOŠNIK[3,4], B. MAVRIČ[1] AND R. VERTNIK[1,5]

[1] Institute of Metals and Technology, Lepi pot 11, SI-1000 Ljubljana, Slovenia, e-mail: bozidar.sarler@imt.si, www.imt.si

[2] University of Nova Gorica, Vipavska 13, SI-5000 Nova Gorica, Slovenia, e-mail: bozidar.sarler@ung.si, www.ung.si

[3] Jožef Stefan Institute, Jamova 39, SI-1000 Ljubljana, Slovenia

[4] Department of Physics, University of Ljubljana, Jadranska 19, SI-1000 Ljubljana, Slovenia

[5] Štore Steel, d.o.o., Železarska cesta 3, SI-3220 Štore, Slovenia

Key words: Solidification, Low Frequency Electromagnetic DC Casting, Multi-Scale Model, Multi-Physics Model, Coupled Problem, Meshless Methods.

Abstract. Simulation and control of macrosegregation, deformation and grain size under electromagnetic (EM) processing conditions is important in industrial solidification systems, since it influences the quality of the casts and consequently the whole downstream processing path. Respectively, a multiphysics and multiscale model is developed for solution of Lorentz force, temperature, velocity, concentration, deformation and grain structure of the casts. The mixture equations with lever rule, linearized phase diagram, and stationary thermoelastic solid phase are assumed, together with EM induction equation for the field imposed by the low frequency EM field or Ohm's law and charge conservation equation for stationary EM field. Turbulent effects are incorporated through the solution of a low-Re turbulence model. The solidification system is treated by the mixture-continuum model, where the mushy zone is modeled as a Darcy porous media with Kozeny-Karman permeability relation and columnar solid phase moving with the system velocity. Explicit diffuse approximate meshless solution procedure [1] is used for solving the EM field, and the explicit local radial basis function collocation method [2] is used for solving the coupled transport phenomena and thermomechanics fields. Pressure-velocity coupling is performed by the fractional step method [3]. The point automata method with modified KGT model is used to estimate the grain structure [4] in a post-processing mode. Thermal, mechanical, EM and grain structure outcomes of the model are demonstrated for low frequency EM casting of round aluminium billets. A systematic study of the complicated influences of the process parameters on the microstructure can be investigated by the model, including intensity and frequency of the electromagnetic field.

1 INTRODUCTION

Direct-Chill (DC) casting [5] turns out to be an efficient technology for production of aluminium semi-products. The process is robust and relatively simple, however it can induce a spectra of defects in the ingots. The control of the process, depending on the product geometry and alloy composition, basically relies on adjusting the mould level, the casting speed, the melt temperature, and the intensity of the water jets that chill the ingot. These control parameters indirectly influence the melt flow and thus the solidification characteristics. An additional handle that can directly affect the flow is offered by alternating EM fields [6], applied to the DC process by means of coils placed around the casting system. They induce the eddy currents in the melt and the ingot that dissipate heat and, more importantly, assert Lorentz force on them, thus providing a stirring force on the melt. A pioneering study of applying low frequency electromagnetic field to the casting process was presented in [7], while a recent magnetohydrodynamic study of this problem was done by our group in [8]. The main aim of the present paper is the extension of this model for including macrosegregation, mechanical effects and grain structure and thus forming a reasonably complete basic multiphysics and multiscale model of the process for the axisymmetric billets.

2 MACROSCOPIC MODELS

2.1 Thermofluid equations

We express all the governing macroscopic transport equations in cylindrical coordinates (r,z), with base vectors $\hat{\mathbf{e}}_r$ and $\hat{\mathbf{e}}_z$ with z coordinate opposite to the casting direction. We limit ourselves to the cases where velocity vector points in the $r-z$ plane. The mixture continuum concept [9], adjusted to DC casting with columnar only solid phase [10] is adopted. The momentum conservation accounts for the Darcy drag term, and the volume force, decomposed into thermal and solutal Boussinesq buoyancy term and the Lorentz force:

$$\rho_m \frac{\partial}{\partial t}\left(\mathbf{v}_m\right)+\rho_m \nabla\cdot\left(\mathbf{v}_m\mathbf{v}_m\right)=-\nabla P_l+\nabla\cdot\left(\mu_l\frac{\rho_m}{\rho_l}\nabla\mathbf{v}_m\right)-\frac{\mu_l}{K}\frac{\rho_m}{\rho_l}\left(\mathbf{v}_m-\mathbf{v}_{\text{cast}}\right)+\mathbf{b} \tag{1}$$

$$\mathbf{b}=-\rho_l\left[\beta_{T,l}\left(T-T_0\right)+\sum_{i=1}^{n}\beta_{C,l}\left(C_l^i-C_0^i\right)\right]\mathbf{g}+\left\langle\mathbf{b}_{\text{EM}}\right\rangle \tag{2}$$

The latter is denoted by $\left\langle\mathbf{b}_{\text{EM}}\right\rangle$ and will be detailed in the following section. The solid phase velocity $\mathbf{v}_S$ is assumed to be constant and equal to the casting velocity $\mathbf{v}_s=\mathbf{v}_{\text{cast}}$, that is parallel to the z coordinate. The mixture density and velocity is defined as $\rho_m=f_l\rho_l+f_s\rho_l$, $\mathbf{v}_m=\left(f_l\rho_l\mathbf{v}_l+f_s\rho_s\mathbf{v}_s\right)/\rho_m$, with f_l and f_s standing for the volume fraction of the liquid and solid phase, respectively. Mass conservation thus reads $\nabla\cdot\mathbf{v}_m=0$. The permeability constant of the Darcy term, relevant in the mushy zone, is modelled as $K=K_0 f_L^3\left(1-f_L\right)^{-2}$ and is put to 0 by hand below the consolidation temperature corresponding to $f_l^{\lim}$, where the liquid phase becomes trapped within the dendrites. The heat and species transfer is formulated with

the mixture convection-diffusion equations:

$$\frac{\partial}{\partial t}\left(\rho_m h_m\right)+\nabla\cdot\left(\rho_m h_m \mathbf{v}_m\right)=\nabla\cdot\left(\lambda_m\nabla T\right)-\nabla\cdot\left[\rho_m\left(h_l-h_m\right)\left(\mathbf{v}_m-\mathbf{v}_{\text{cast}}\right)\right] \tag{3}$$

$$\begin{aligned}&\frac{\partial}{\partial t}\left(\rho_m C_m^i\right)+\nabla\cdot\left(\rho_m C_m^i \mathbf{v}_m\right)=\\&=\nabla\cdot\left(\rho_m f_l D_l^i\nabla C_m^i\right)+\nabla\cdot\left[\rho_m f_l D_l^i\nabla\left(C_l^i-C_m^i\right)\right]-\nabla\cdot\left[\rho_m\left(C_l^i-C_m^i\right)\left(\mathbf{v}_m-\mathbf{v}_{\text{cast}}\right)\right]\end{aligned} \tag{4}$$

The enthalpy of the mixture is defined as $h_m=f_l h_l+f_s h_s$, where the constitutive relations are given as $h_S(\mathrm{T})=\rho_s c_{ps} T$ and $h_l(T)=\rho_l\left[c_{ps}T+c_{pl}(T-T_{sol})\right]+h_M$, with h_M denoting melting enthalpy. We assume that f_l rises consistent with the Lever rule in the mushy zone, $T>T_{liq}\left(C_m^i\right): f_l=1,\quad C_l^i=C_m^i;\ T_{liq}\left(C_m^i\right)\geq T\geq T_{sol}\left(C_m^i\right): C_m^i=\left(1-f_l\right)k^i C_l^i,\ T=T_{liq}\left(C_l^i\right); T<T_{sol}\left(C_m^i\right): f_l=0$, $C_l^i=C_m^i/k^i$ and that the heat conduction is a weighted average $\lambda=f_l\lambda_l+f_s\lambda_s$. On the inlet boundary (north) of the axisymmetric domain we impose the fully developed Poisseuille flow profile with known casting temperature and nominal concentration of the alloying elements C_0^i:

$$\mathbf{v}_S=\mathbf{v}_L=-\hat{\mathbf{e}}_z v_{cast}\frac{2R^2}{R_{inlet}{}^2}\left(1-\frac{r^2}{R_{inlet}{}^2}\right),\quad T=T_{cast} \tag{5}$$

where R_{inlet} and R are the inlet and mould radii, respectively. On the top free surface we set the temperature to the casting temperature and concentration to the nominal alloy concentration, and for the velocity, we set $\partial v_r/\partial z=0, v_z=0$. On the left (symmetry) boundary, we prescribe $v_r=0,\ \partial v_z/\partial r=0,\ \partial T/\partial r=0, C_l^i=C_0^i$. On the right boundary (cooling side), the sticking boundary condition in the moving system is $\mathbf{v}=-v_{\text{cast}}\hat{\mathbf{e}}_z$. The cooling side temperature boundary condition is modelled with the Robin boundary condition $-k\partial T/\partial r=h(z)\left(T-T_{env}\right)$, where $h(z)$ takes into account variation of the heat transfer coefficient with coordinate . It vanishes in the hot-top region. In the mould chill region we set it to a constant value h_{MC} whereas in the direct chill region it starts at value h_{DC} just below the mould chill and linearly rises to $3h_{DC}$ on the bottom of the direct chill region. Finally, on the bottom boundary we require constant field derivatives in the casting direction $\partial T/\partial z=0,\ \partial v_z/\partial z=0,\ v_r=0,\ \partial C_l^i/\partial z=0$.

2.2 Electromagnetic field equations

The dynamical pair of Maxwell is:

$$\nabla\times\mathbf{E}=-\frac{\partial\mathbf{B}}{\partial t},\quad \nabla\times\mathbf{B}=\mu_0\mathbf{J}+\frac{1}{c^2}\frac{\partial\mathbf{E}}{\partial t},\quad \left(\mu_0=4\pi\times10^{-7}\,\mathrm{Vs/Am}\right) \tag{6}$$

where we assume $c=\infty$ and work in the quasi-static approximation. Electric $\mathbf{E}$ and magnetic $\mathbf{B}$ fields are both divergence-free, i.e., solenoidal. In addition, the Ohm's law in the

moving frame relates fields with induced eddy currents, $\mathbf{J}=\sigma\left(\mathbf{E}+\mathbf{v}\times\mathbf{B}\right)+\mathbf{J}_{ext}$, where σ is conductivity that is nonzero only in the conductor, whereas $\mathbf{J}_{ext}$ is nonzero only in the coil and can be viewed as a boundary condition. We work with the electromagnetic potential $\mathbf{A}$ defined through $\mathbf{E}=-\nabla\phi-\partial\mathbf{A}/\partial t$, $\mathbf{B}=\nabla\times\mathbf{A}$ and impose the Coulomb gauge, $\nabla\cdot\mathbf{A}=0$, for the vector potential. Maxwell equations thus reduce to induction equation for $\mathbf{A}$:

$$\nabla^2\mathbf{A}=\mu_0\sigma\left(\frac{\partial\mathbf{A}}{\partial t}-\mathbf{v}\times\nabla\times\mathbf{A}\right)-\mu_0\mathbf{J}_{\text{ext}},\ \ \phi=0 \tag{7}$$

We set $\mathbf{v}=0$ on the right-hand side since the effect of velocity on the EM field is small in regime of small magnetic Reynolds number. Details of equations in axisymmetry are given in [8].

2.3 Solid mechanics equations

The solid mechanics model is solved by assuming the calculated temperature field from the thermal model. The assumed thermoelastic governing equation is:

$$G\nabla^2\mathbf{u}+(G+\lambda)\nabla\nabla\cdot\mathbf{u}+\nabla\lambda\nabla\cdot\mathbf{u}+\nabla G\left(\nabla\mathbf{u}+\left(\nabla\mathbf{u}\right)^T\right)=\nabla\left(\beta_T\left(T-T_{ref}\right)\right)-\mathbf{f} \tag{8}$$

where G stands for shear modulus, λ for Lamé parameter and $\mathbf{f}$ is the body force. The coupling with the temperature field is described by the coefficient β defined as $\beta=(3\lambda+2G)\alpha$ which is composition dependent. Another free parameter is the reference temperature T_{ref}, which denotes the temperature at which the thermal expansion is considered to be zero.

3 MICROSCOPIC MODEL

The microscopic model is solved in a post-processing mode. The model inputs temperature and concentration data from the macroscopic model. The representative input data are taken from the billet center, middle and surface streamlines in Lagrangean sense. The time for microscopic model is calculated from the velocity and length of the streamline. A typical 3x3mm representative traveling area is considered on each of three considered streamlines.

3.1 Nucleation kinetics

To describe the nucleation event the continuous Log-normal Nucleation model is adopted. The variation of the grain distribution in each time step depends on the undercooling temperature in the bulk of the casting. The density of grains $n\left(\Delta T_{nuc}\right)$ at the given degree of undercooling ΔT_{nuc} is given by the integral of nucleation density distribution:

$$\frac{dn}{d\Delta T_{nuc}}=\frac{n_{\max}}{\sqrt{2\pi}\Delta T_\sigma}\frac{1}{\Delta T_{nuc}}\exp\left[-\frac{1}{2}\left(\frac{\ln\Delta T_{nuc}-\ln\Delta T_0}{\Delta T_\sigma}\right)^2\right] \tag{9}$$

where ΔT_0, ΔT_σ, $n_{\max}$ represent the mean nucleation undercooling, the standard deviation and the maximum density of nuclei that can form in the melt, respectively. These three

standard nucleation parameters are determined experimentally for each alloy and grain refiner by measuring the grain size.

3.2 Grain growth kinetics

A modified KGT model is used to predict the grain growth velocities. The growth process is driven [11] by the local undercooling, approximated from the linearized phase diagram of a multicomponent alloy $\Delta T = T_{liq} - T(t) + \sum_{i=1}^{n} m_i \left(C_l^i - C_0^i \right)$, where T_{liq}, T, m_i, C_l^i, C_0^i represent the liquidus temperature, the temperature recalculated from the macro model, the liquidus slope of species i, the liquid concentration of species recalculated from the macro model and the initial concentration of species i. In order to calculate the grain velocity V, the transport equations are solved for each species i. The solution relates the nondimensional supersaturations for each alloying element i, to the corresponding growth Péclet number $\Omega_i = F(P_i)$, $P_i = rV / 2D_i^l$ where r is a tip radius. The supersaturation Ω_i is expressed by the Ivantsov function for the purely diffusive growth regime $F(P_i) = \mathrm{P}_i \exp(\mathrm{P}_i) E_1(\mathrm{P}_i)$ where E_1 is the integral exponential function. The total undercooling can be expressed as:

$$\Delta T = \sum_{i=1}^{n} m_i C_0^i \left(1 - \frac{1}{1 - (1 - k_i) F(P_i)} \right) \tag{10}$$

where k_i is the partition coefficient of species i. The marginally stable plane front solution is applied in order to select the solution $V(\Delta T)$, with $r = V^{-1/2} \sqrt{4\pi^2 \Gamma / \sum_{i=1}^{n} m_i (k_i - 1) C_l^i / D_i^l}$, where Γ stands for the Gibbs-Thomson coefficient.

4 SOLUTION PROCEDURES

The time-averaged Lorentz force is calculated by discretizing the calculation domain in local domains with 9 nodes with the approximation function expressed as a minimum least squares fit of 6 monomials $\left(1, x, y, xy, x^2, y^2\right)$. The weight function in the least squares problem is chosen to be Gaussian, $e^{-|\mathbf{r}|^2/\xi}$. ξ is an average squared distance from the center node to all nodes in the local domain. The sparse linear system is solved using the sparse system solver [12]. The EM field calculation domain extends $1.5H$ beyond the casting system in vertical direction and is terminated at $3R$ in the radial direction. Unstructured node arrangement is used for the EM field calculation that has embedded the nodes for the thermofluid equations in a way that in the mould the EM and thermofluid nodes coincide. The transport equations for mass, momentum, energy, and concentration are solved by collocation with multiquadrics radial basis functions with 5-noded subdomains in case of thermal model (as described in [13, 14]) and 6-noded subdomains in case of mechanical model as elaborated in the present proceedings [15].

The phase change kinetics equations are solved by the PA method. The representative microscopic calculated domain with a dimension 3x3 mm is discretized into 360 000 randomly located nodes. The post processing calculations of temperature and concentration

for this domain are taken from the macro level of calculations. The details of the PA method are elaborated in [16]. The potential nucleation sites are randomly located in this domain in each time step. The newly arisen site represents a new family and gets a randomly chosen color at the time when it appears. As grains nucleate, they start to grow with respect to the PA neighborhood configuration which is associated with the position of the neighboring PA nodes which fall into a circle with assumed radius $R_h = 0.5\,\mu\text{m}$. Due to random arrangement of the nodes each grain gets different neighboring configuration. For the given values of the physical and thermodynamic properties m_i, k_i, D_l^i of each alloy element i, the variable grain growth velocity V for a specified undercooling temperature ΔT can be calculated. Independent calculations of the growth velocity for a given set of these values are carried out in each time step by using an iterative method. This requires to provide the micro model with values of T and C_l^i, taken from the macro model at every 0.05 s.

5 NUMERICAL EXAMPLES

Six cases of aluminium (Al-Cu-5.25%) alloy were simulated, where the majority of the casting parameters remained constant. These parameters are shown in Table 1. Other parameters (casting speed, EM amplitude, EM frequency) were varied in order to study their effect on the shape and dimension of the liquid sump. Overview of calculated cases is given in Table 2.

Table 1: Casting parameters.

Casting temperature	707 °C
Cooling water flow	140 m^3/h
Liquidus temperature	643 °C
Solidus temperature	562 °C
Liquid thermal conductivity	88.1 W/mK
Solid thermal conductivity	180 W/mK
Liquid specific heat	1160 J/kgK
Solid specific heat	1270 J/kgK
Permeability constant	$6.7 \cdot 10^{-11}$ m^2
Latent heat	$3.0 \cdot 10^5$ J/kg
Billets on a table	20
Number of coil turns	48
Coil width	20 mm
Coil height	80.97 mm
Coil inner radius	187.5 mm
Coil lowest point	-101.87

Table 2: Cases descriptions.

Case number	Casting speed	Amplitude	Frequency
Case 1	60 mm/min	0	0
Case 2	80 mm/min	0	0
Case 3	100 mm/min	0	0
Case 4	80 mm/min	10 A	10 Hz
Case 5	80 mm/min	10 A	15 Hz
Case 6	80 mm/min	10 A	20 Hz

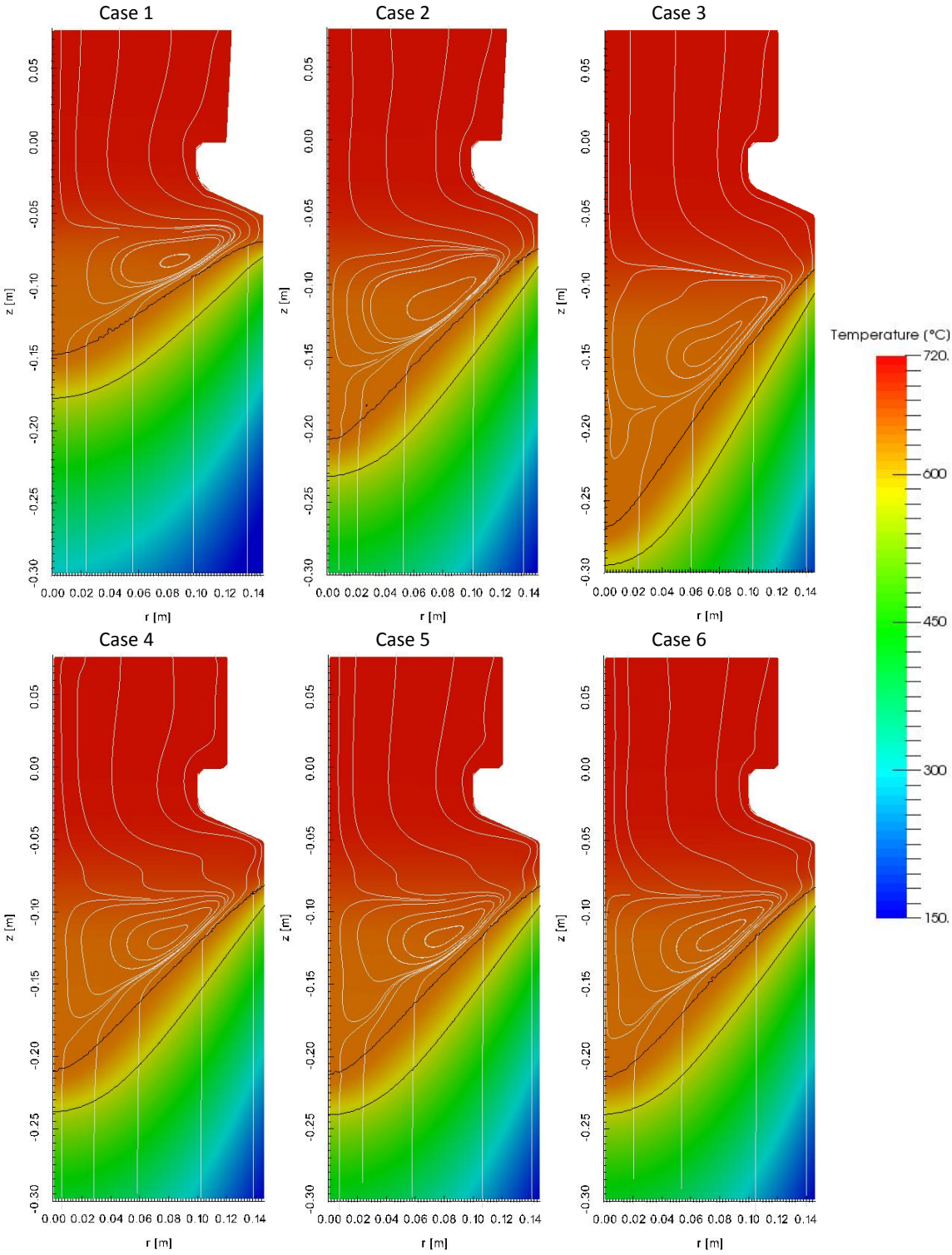

Figure 1: Temperature distribution and streamlines are shown for cases 1 - 6.

The effect of the casting speed is evident from the comparison of results of cases 1, 2 and 3, where the casting speed has values of 60, 80 and 100 mm/min respectively. It is obvious that an increase in velocity will result in deeper billet sump, which is in accordance with general observations in DC casting. The depth of the sump (solidus line at the center) increases as 18 cm, 23 cm, 29.5 cm in cases 1, 2 and 3 respectively. Furthermore, the thermo-solutal eddy in the central portion of the billet is also increasing with the casting speed.

Case 2 (no EM field) and cases 4, 5 and 6 (with EM field) can be compared to observe the effect of the EM field on the DC casting, as all cases were calculated for the same non EM field related casting parameters. Even though the sump depth is slightly smaller in the case of EM field, larger differences can be observed in the velocity field. The eddy formed in the sump due to natural convection is smaller in case 5. The streamlines are shallower, as the EM force amplifies the velocity in the horizontal direction.

As the frequency is relatively small (low frequency EM casting) in all three simulated cases accounting the EM field, the differences in the sump shape are barely visible. Nevertheless, the effect of electromagnetic frequency variations can be noticed from the streamlines, especially in the zone above the central eddy. If the EM frequency is increased, the streamlines of the inlet melt flow become more parallel with billet axes. Furthermore, higher frequency causes flatter central eddy.

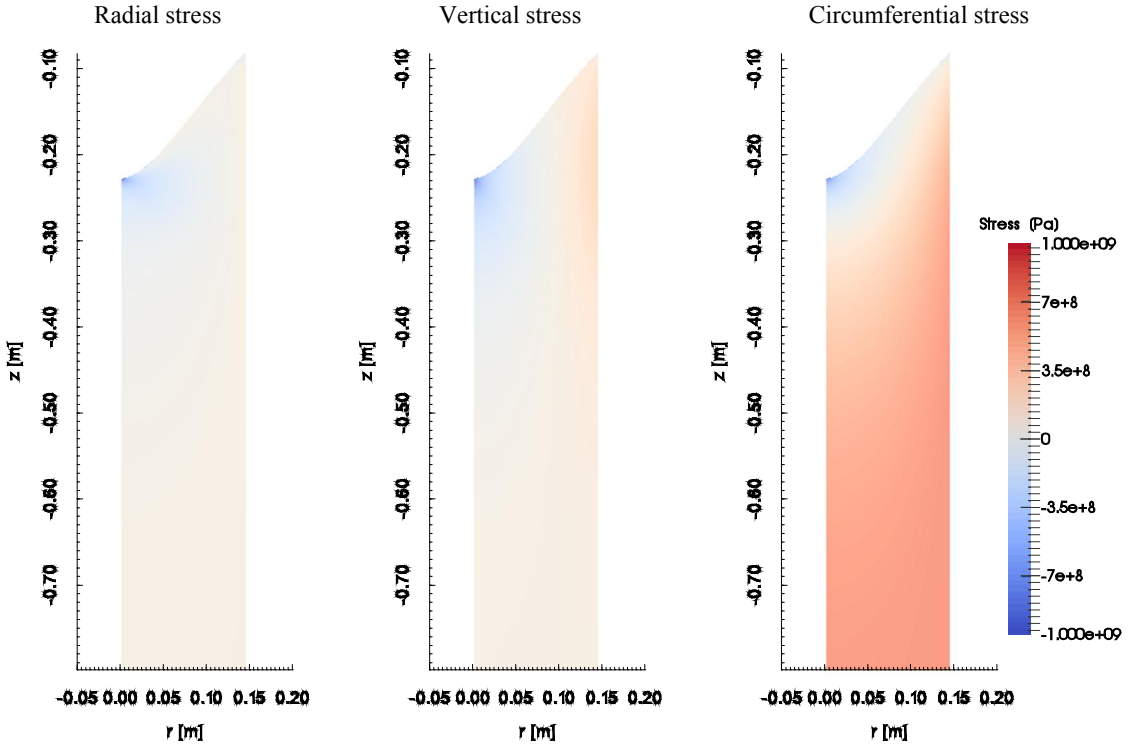

Figure 2: Stress calculations from the thermoelastic model for case 4.

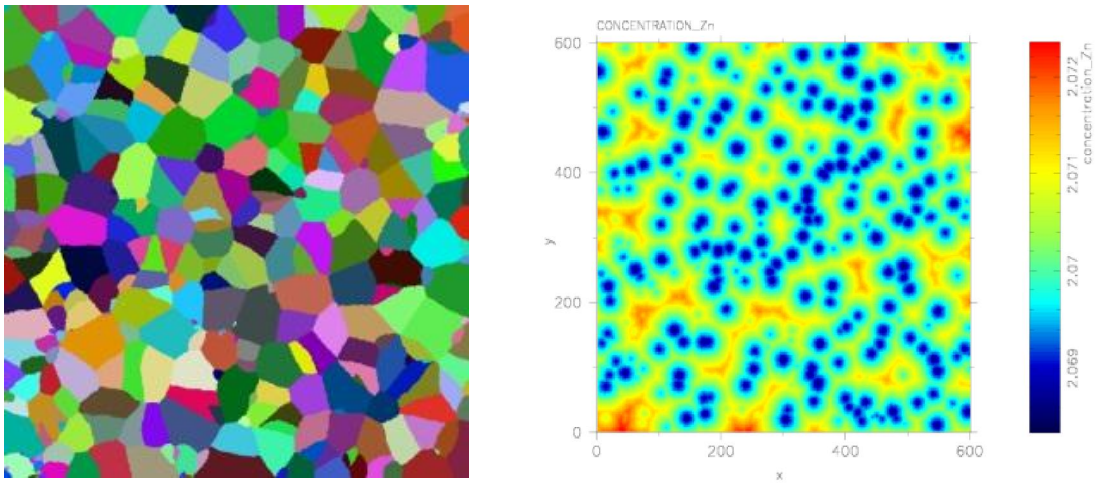

Figure 3: Results from the grain structure model: structure and Zn concentration for Al-Zn--5.35% Mg-2.35% Cr-1.5% Cu-0.5% alloy.

6 CONCLUSIONS

A reasonably complete coupled multiphysics and multiscale model of the low frequency electromagnetic casting has been developed. First the electromagnetic field is calculated, followed by the calculations of the momentum equation, pressure velocity-coupling, the energy equation, and species equations, respectively. The mechanical calculations are performed without feedback, based on the thermal calculations. The microstructure calculations are coupled in Lagrangean sense to the calculated velocity and concentration fields in a post-processing mode. The models are on the macro level solved by the diffuse approximate method and on the micro-level by the point automata method. This novel approach is completely meshless and no polygonisation is needed. The considered physical models incorporate only simple, basic elements that obviously need further improvements. In the field of macrosegregation, the movement of the solid phase and influence of the grain refiner represent the next necessary steps [17]. In the field of solid mechanics, the introduction of viscoelastic behavior and feedback to the thermal model (mould heat transfer) seems important. In the field of microstructure modelling, the inclusion of the secondary phases is necessary in the model. It should be pointed out that the extension of the present numerical approach to three dimensions seems straightforward, since the coding of the present axisymmetric meshless formulation is equivalent in higher dimensions. The capabilities of the model were demonstrated in figures 1, 2 and 3.

ACKNOWLEDGEMENTS

Support from the Slovenian Grant Agency in the framework of the project L2-6775 and young researchers grants, Slovenian Ministry for Economy in the framework of the Voucher projects and IMPOL Aluminium Industry is kindly acknowledged.

REFERENCES

[1] Vertnik, R., Založnik, M. and Šarler, B. *Eng.Anal.Bound.Elem.* (2006) **30** 847-55.
[2] Šarler, B. and Vertnik, R. *Comput. Math. Appl.* (2006) **51** 1269-82.
[3] Chorin, A. J. *J. Comput. Phys*. (1967) **2** 12-26.
[4] Lorbiecka, A. Z. and Šarler, B. *Materials Science Forum* (2014) **790-791** 115-20.
[5] Eskin, D. G. *Physical Metallurgy of Direct Chill Casting of Aluminium Alloys*. Boca Raton: CRC Press/Taylor & Francis (2008).
[6] Davidson, P. A. *An Introduction to Magnetohydrodynamics*. Cambridge: Cambridge University Press (2001).
[7] Dong, J. and Cui, J. Z. *Metall. Mater. Trans*. (2004) **35A** 2487-95.
[8] Košnik, N., Vertnik, R. and Šarler, B. *Materials Science Forum* (2004) **790-791** 390-395.
[9] Bennon, W. D. and Incropera, F. P. *Numer. Heat Transf.* (1988) **13A** 277-96.
[10] Du, Q., Eskin, D. G. and Katgerman, L. *Metall. Mater. Trans.* (2007) **38A** 180-89.
[11] Appolaire, B., Combeau, H. and Lesoult, G. *Mater. Sci. Eng. A* (2007) **487** 33-45.
[12] Schenk, O. and Gärtner, K. *Journal of Future Generation Computer Systems* (2004) **20** 475-487.
[13] Kosec, G., Založnik, M., Šarler, B. and Combeau, H. *Comput. Mater. Cont.* (2011) **22** 169-59.
[14] Kosec, G. and Šarler, B. *Eng. Anal. Bound. Elem.* (2014) **45** 36-44.
[15] Mavrič, B. and Šarler, B. *ICASP-4 Proceedings* (2014) (to appear)
[16] Lorbiecka, A. Z. and Šarler, B. *CMC* (2010) **18** 69-104.
[17] Nadella, R., Eskin, D. G., Du, Q. and Katgerman, L. *Progress in Materials Science* (2008) **53** 421-480.